Progress In Electromagnetics Research C, Vol. 84, 61–74, 2018

Compact UWB MIMO Antenna with Metamaterial-inspired Isolator

Fei Wang*, Zhaoyun Duan, Shifeng Li, Zhanliang Wang, and Yubin Gong

Abstract—In this paper, a dual-band complementary split ring resonator (C-SRR) is used to improve the band-notch effect relative to the traditional SRR. Meanwhile, we employ a brand-new SRR unit cell as an isolator for decoupling *among multiple* bands without enlarging the dimensions of the multiple-input-multiple-output (MIMO) antenna. Therefore, a compact ultra-wideband MIMO antenna is developed. Compared with the previous work, the proposed MIMO antenna also has obvious advantages such as high isolation and miniaturization (the dimensions are only 13.5 mm × 34 mm). The metamaterial-inspired UWB MIMO antenna presented here is suitable for small scaled mobile devices.

1. INTRODUCTION

With the rapid development of wireless communications and the demands for high transmission rate and stable transmission quality, multiple-input-multiple-output (MIMO) technology has been widely employed [1, 2]. MIMO antennas use multiple antenna elements for transmitting and receiving signals in the wireless communication systems. The MIMO technology can improve the capacity of the communication system and the utilization ratio of the spectrum without increasing the transmitting power.

Ultra-wideband (UWB) technology is used for short range wireless communication among multiple devices. UWB systems operate under a low power level (41.3 dBm/MHz) within a wide operation band (3.1 GHz–10.6 GHz) [3–5]. Since the UWB system operates at such a wide spectrum that covers many communication systems, it is necessary to find an efficient method to reduce the signal interference between the UWB system and other wireless communication systems. Despite of the utilization of the slots on the patch and/or on the ground to achieve the band-notch effects, other problems, such as high loss of the antenna radiation efficiency and reflection coefficient, still exist. So far, several studies of the applications of the MIMO technology to the UWB system have been done for enhancing the system stability [6, 7]. However, the problem of realizing high isolation in the whole operating spectrum within a compact structure is serious, and plenty of studies have been done. Zhang et al. used the tree-like structure which resonates at multiple frequencies to reduce the mutual coupling [8]. Liu et al. proposed a compact UWB MIMO antenna, and the orthogonal polarization is used for enhancing isolation [9]. Chacko et al. utilized both tree-like structure and orthogonal polarization for decoupling [10]. Iqbal et al. used F-shaped stubs to realize low mutual coupling with high gain [11].

Metamaterial has been widely used in the antenna field due to its unique electromagnetic characteristics. The researches show that the metamaterial can be used for improving the antenna performance such as enhancing radiation properties [12], extending bandwidth [13], reducing mutual coupling [14], miniaturization [15], band-notching [16, 17], and multiple bands realization [18]. In recent years, some attempts using metamaterials such as electromagnetic band gap [19], single negative materials [20], and artificial magnetic conductor [21, 22] to realize high isolation in the MIMO antennas

Received 2 March 2018, Accepted 30 April 2018, Scheduled 15 May 2018

* Corresponding author: Fei Wang (wfken231@163.com).

The authors are with the School of Physical Electronics, University of Electronic Science and Technology of China, Chengdu, China.

Table 1. Dimensions of the UWB antenna.

Symbol	Parameters (unit: mm)
W	15
L	25
gw	8
gl	13
al_1	10
al_2	6
f_1	4
f_2	4
aw	4
fw	1
sw	1

have been made. In these studies, an array of metamaterials is employed for decoupling only at a single frequency while the metamaterial array unavoidably leads to large bulk and difficult fabrication. Furthermore, the studies of using less amount of metamaterial unit have also been reported. Ketzaki and Yioultsis used single SRR unit cell to enhance isolation of the monopole MIMO antenna [23]. Abdalla and Ibrahim proposed the monopole antenna with CRLH structure and defected ground to realize high isolation [24]. In [25], Khan et al. used complementary split ring resonator (C-SRR) to suppress the mutual coupling in UWB MIMO antenna. However, these methods still face challenge in multiple frequencies decoupling.

To solve above problems, we use a dual-band C-SRR similar to that in [27] to improve the band-notch effect. In addition, a novel decoupling split ring resonator (SRR) which resonates at 3 GHz and 9.5 GHz is developed. Only using a single unit cell, the decoupling SRR can realize the high isolation and benefits the miniaturization. Next, a compact co-planar waveguide fed (CPW-fed) dual band-notch UWB MIMO antenna is built and measured. Finally, the correlation coefficient of the UWB MIMO antenna is calculated from the measured results.

2. UWB MIMO ANTENNA

2.1. UWB Antenna Design

In this paper, a CPW-fed UWB antenna is studied. Its geometry is shown in Fig. 1, and its structural parameters are listed in Table 1. The width of the slot between the feedline and ground plane is 0.25 mm. The antenna patch is printed on an FR4_epoxy substrate with the relative permittivity of 4.4 and the loss tangent of 0.02. The substrate is 1 mm thick.

To shrink the size of the proposed antenna, the L-shape ground is adopted, as illustrated in Fig. 1. The equivalent circuit model of the UWB antenna is presented in Fig. 1(b). The L-shape feeding line provides the unbalance feeding line (L_1, C_1 and L_2, C_2) for better impedance matching. The slots between the L-shaped ground and antenna patch can bring extra capacitance (C_{32}, L_{32}, C_{62}, L_{62}, etc. in Fig. 1(b)) for the antenna, which introduces the resonance at lower frequencies. After the optimization as illustrated in Fig. 1(c), the width gw and length gl of the ground slot are set as 8 mm and 13 mm, respectively. Thus, the L-shape ground can increase the electric length of the antenna and reduce the antenna size. Besides, a quarter circle arc patch is added on the antenna patch to extend the bandwidth of the UWB antenna.

2.2. Band-Notch Structure

UWB technology is usually used for indoor short range communication. Therefore, it is necessary to avoid the mutual interference between the UWB system and other wireless communication systems such

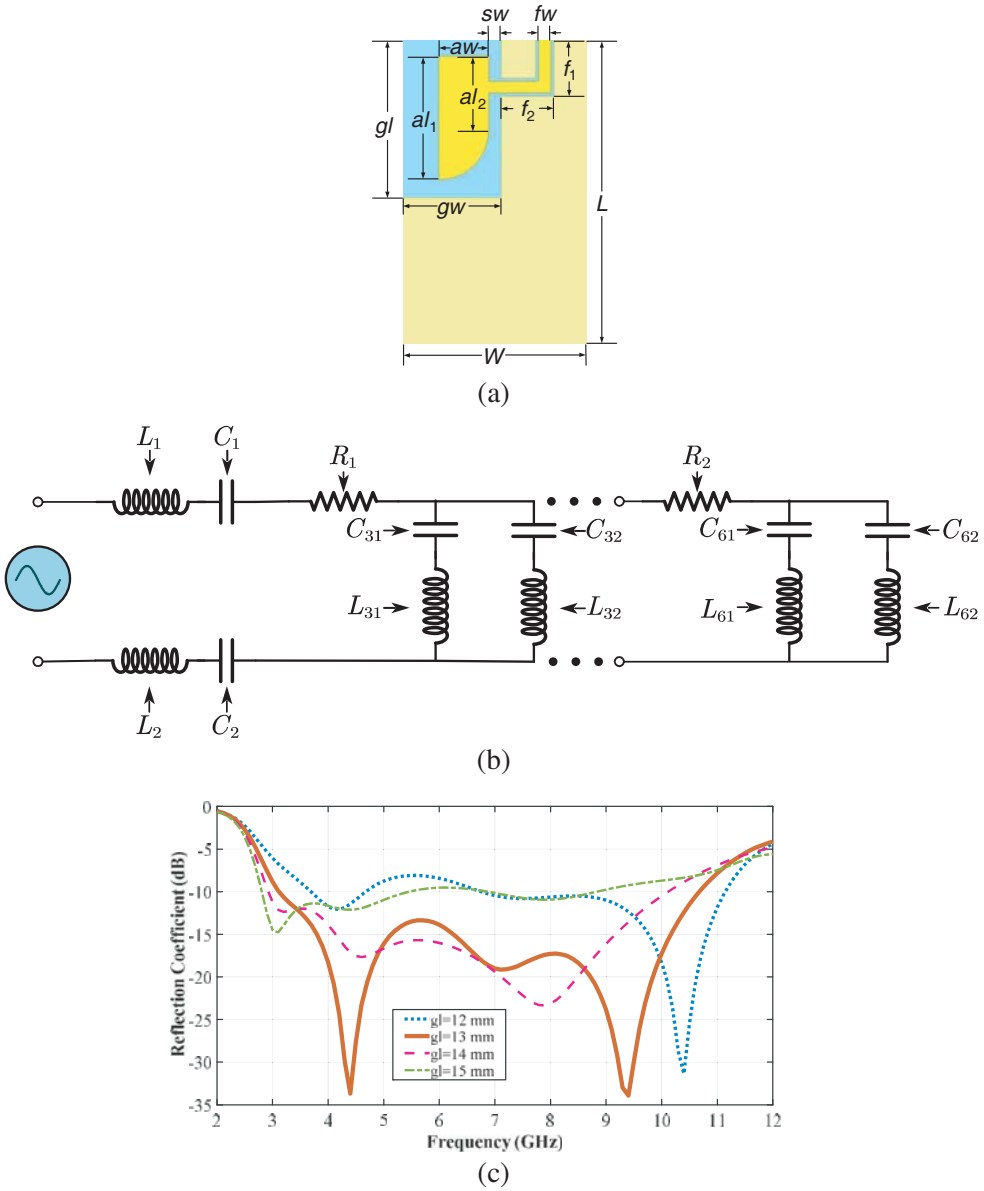

Figure 1. (a) UWB antenna geometry, (b) its equivalent circuit model, and (c) its reflection coefficient with different slot length.

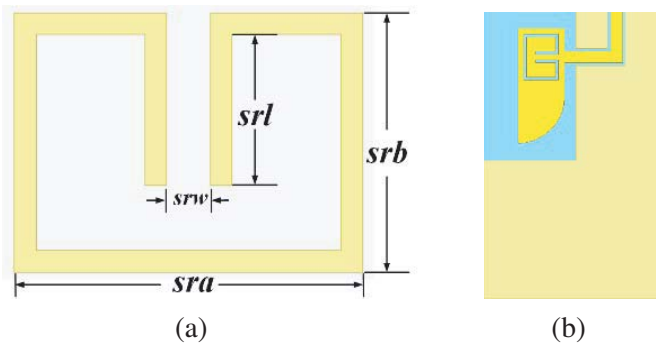

Figure 2. (a) Dimensions of the C-SRR, (b) the UWB antenna with the C-SRR.

Table 2. Dimensions of the C-SRRs.

Symbol	Parameters (unit: mm)
sra	3
srb	4
srw	1
srl	2
sra_2	5
srb_2	7
srw_2	1
srl_2	2.5

as W-LAN (around 5.8 GHz) and Wi-MAX (around 3.55 GHz) systems. To achieve band-notch features with less influence on antenna performance, we load C-SRRs as a band-notch structure into the UWB antenna. A 5.80 GHz C-SRR is designed, as shown in Fig. 2(a). The parameters of the C-SRR are listed in Table 2, and slots' width is 0.5 mm. The geometry of the UWB antenna is presented in Fig. 2(b).

To further enhance the band-notch effect, a new C-SRR similar to that in [27] has been adopted. Here we modify the C-SRR structure to strength its resonance at higher frequencies for dual band-notches and then further investigate the dual-band properties of this new C-SRR.

The dimensions of the new C-SRR are presented in Table 2. Its structure and S-parameters are shown in Figs. 3(a) and (b), respectively. From Fig. 3(b), it is observed that the dual-band C-SRR resonates at both 3.55 and 5.80 GHz which means that the C-SRR etched on the antenna can help improve the band-notch effect at both frequencies. The electric field distributions on the C-SRR both at 3.55 GHz and 5.80 GHz are presented in Figs. 3(c) and (d), respectively. From the figures, it can be seen that the C-SRR provides a resonance at higher frequency (around 5.80 GHz) and the SRR-like structure provides another resonance at lower frequency (around 3.55 GHz). The extracted effective parameters of the dual-band C-SRR are presented in Figs. 3(e) and (f). It can be found that the dual-band C-SRR behaves as negative permittivity (ENG) at 3.55 GHz and negative permeability (MNG) at 5.8 GHz. As shown in Fig. 3(f), since the resonance is weak at 5.8 GHz, the 5.80 GHz C-SRR is retained to guarantee the band-notch effect.

When etching the new C-SRR on the ground plane, the final geometry of the UWB antenna is presented in Fig. 4(a), and its S_{11} parameters are shown in Fig. 4(b). From Fig. 4(b), it is obvious that the new C-SRR has greatly improved the band-notch effect at both frequencies. The peak values of the $|S_{11}|$ reach -2.5 dB and -3 dB at 3.55 and 5.80 GHz, respectively. The $|S_{11}|$ is larger than -5 dB in the two notch bands. Note that the resonant frequency of this C-SRR will be slightly affected when being loaded in the antenna, but the C-SRR still resonates in the notch band that can ensure the band-notch effect.

2.3. MIMO Antenna Design

Based on the UWB antenna presented above, a two-element UWB MIMO antenna is constructed, as shown in Fig. 5(a). The UWB antenna elements are symmetrically printed on the substrate. Locating two elements on the edges of the substrate can increase the distance between them, thus enhance the isolation. The slot on the middle of the ground plane extends the current path between two ports and is helpful to further improve the isolation. Relative to the single UWB antenna, the extended ground plane of the MIMO antenna can effectively expand the radiation area and improve the radiation performance. Using the optimization tool in HFSS, it can be seen that the best size of the slot width msw and length msl should be 5 mm and 10 mm, respectively.

As shown in Fig. 5(b), due to the extended ground plane, the dimension of single antenna element can be largely reduced. The decrease of the MIMO antenna length will slightly influence its performance once the L-shape ground structure can be ensured. Hence, the length ML and width MW of the MIMO

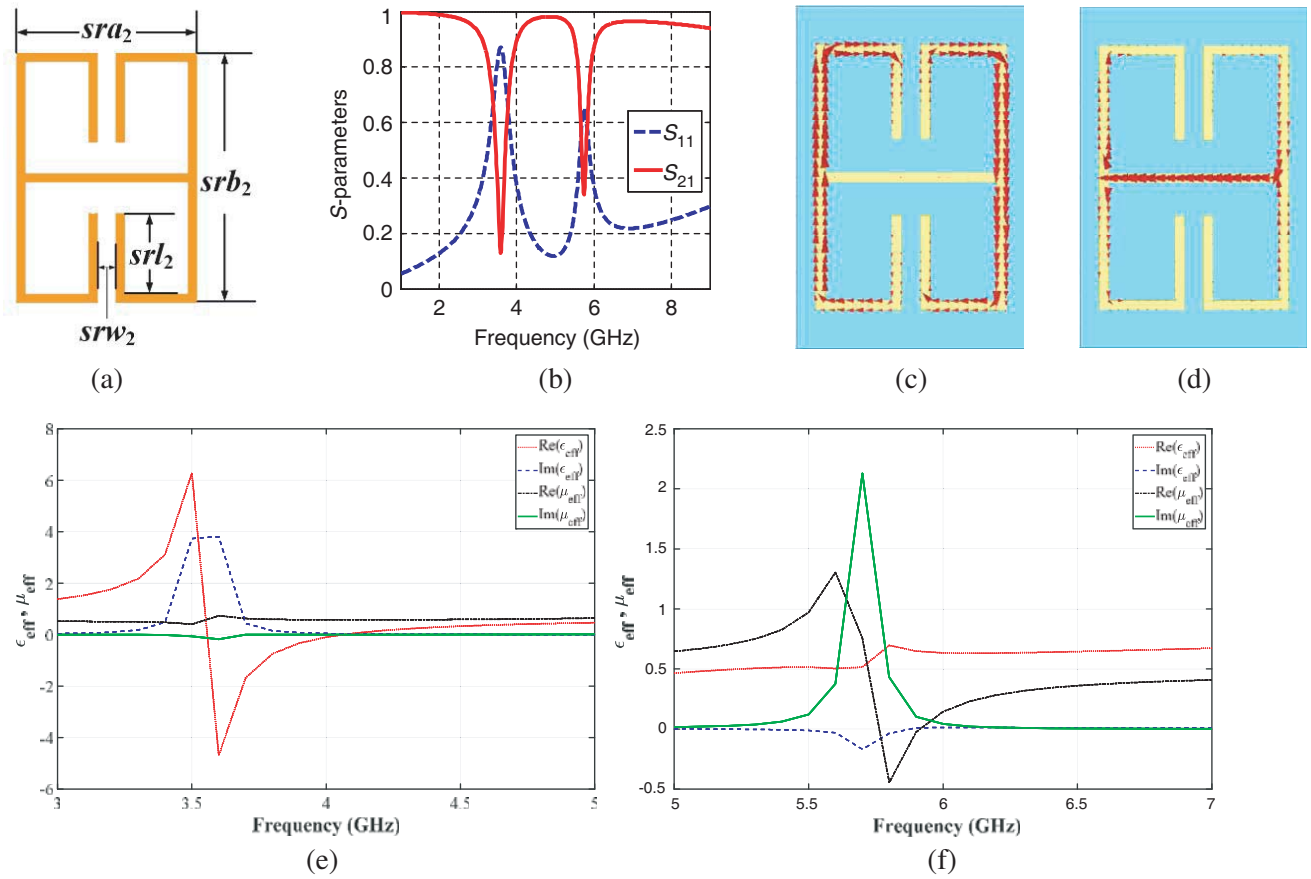

Figure 3. (a) Dual band C-SRR geometry, (b) its normalized S_{11} parameters, (c) surface current distribution on the C-SRR at 3.55 GHz and (d) at 5.80 GHz, the effective parameters of the dual band C-SRR around (e) 3.55 GHz and (f) 5.8 GHz.

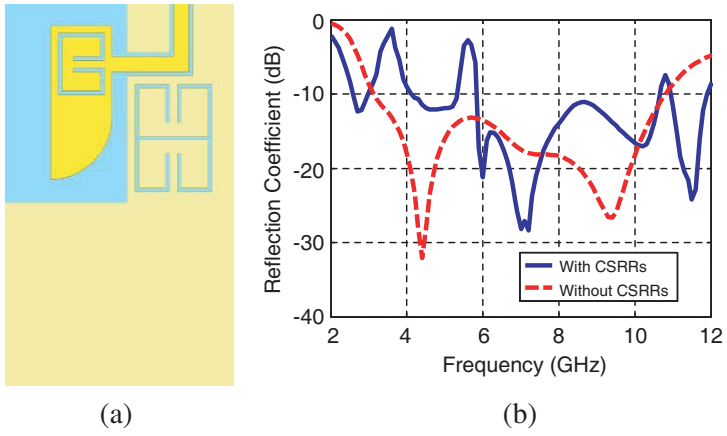

Figure 4. (a) Geometry of the UWB antenna, (b) its S_{11} parameters.

antenna are set as 13.5 mm and 34 mm, respectively. The simulated S-parameters of the MIMO antenna are illustrated in Fig. 5(c). $|S_{11}|$ shows that the band-notch effect is dominant, and the impedance matching is good except for the two notch bands. The $|S_{21}|$ parameters significantly decrease from 3 GHz to 4.5 GHz, and a strong mutual coupling appears from 7 GHz to 11 GHz.

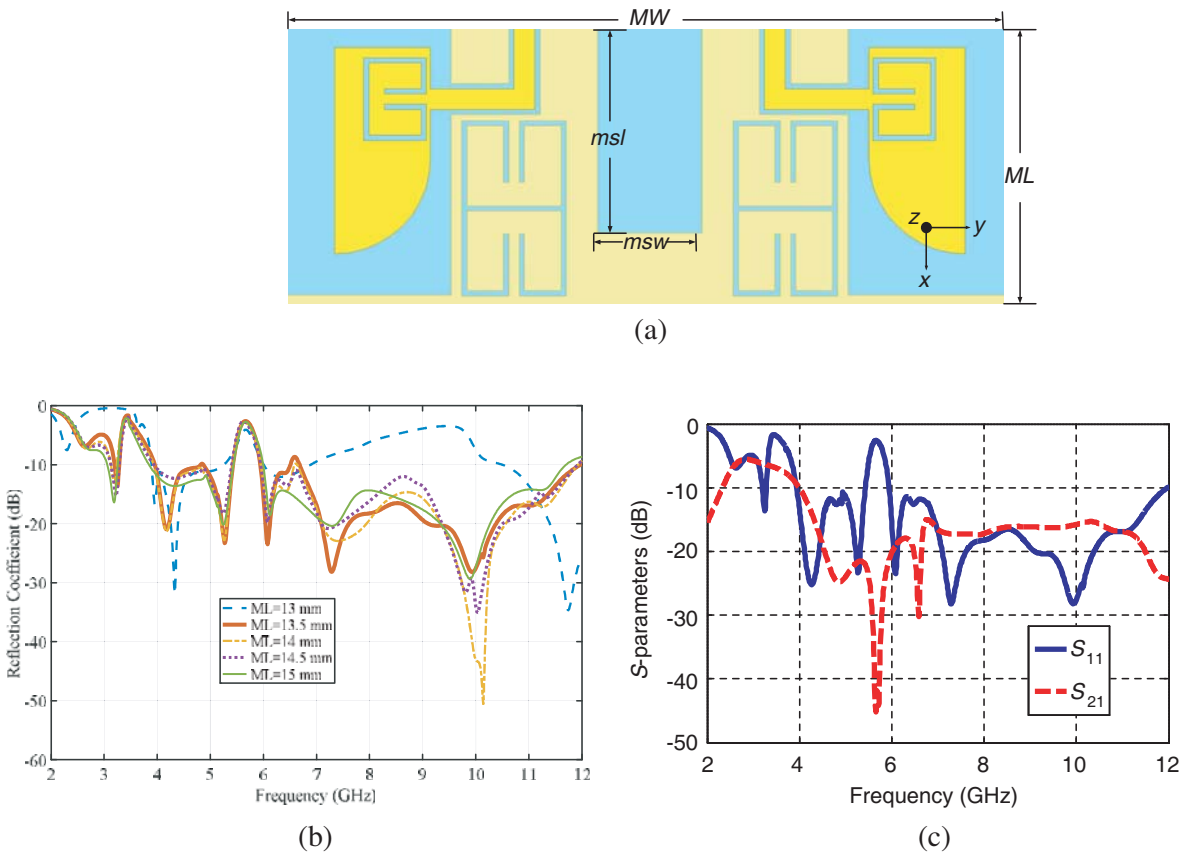

Figure 5. (a) MIMO antenna schematic, (b) the reflection coefficient with different length and (c) its S-parameters.

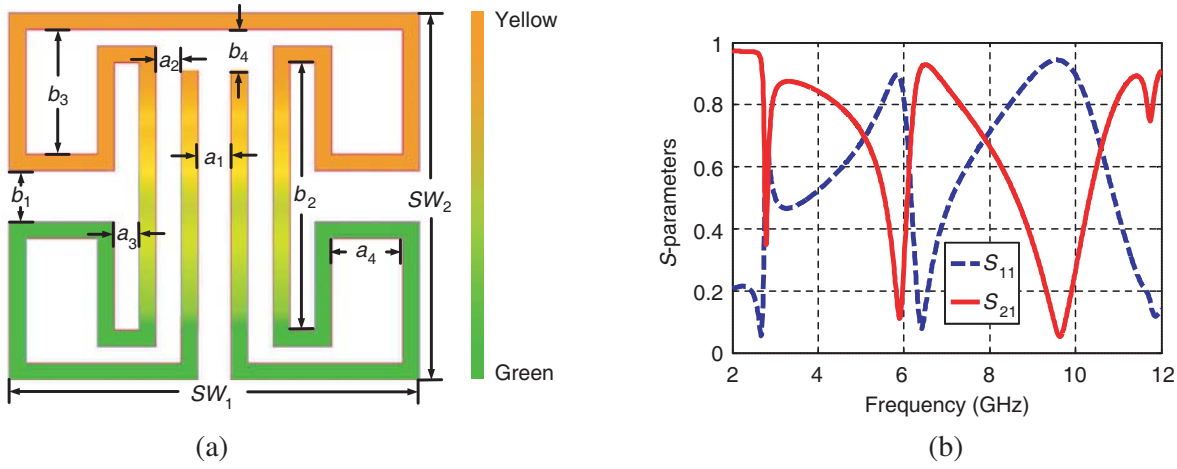

Figure 6. (a) Decoupling SRR schematic and (b) its normalized S-parameters.

3. ISOLATOR DESIGN

In previous studies, the traditional SRR [27] arrays have been used in MIMO antenna design to solve the decoupling problem [19–22]. The SRR array has been used as an effective medium with negative permeability properties in a narrow bandwidth, while in the present study, the size of the proposed antenna is so small that it cannot offer enough space for the metamaterial array. Besides, unlike

the situation in [23–26], the coupling is significant in two bands which means that those traditional SRR cannot fulfill the requirements. Therefore, we use single SRR unit cell as an isolator. Using the simulation software, we analyse the field distribution between the antenna elements and find the area where the coupling energy is centred on. Placing the isolator in this area, the coupling energy will excite a strong resonance on the SRR, and the energy coupled to the antenna patch will be largely reduced.

In line with this, a new type of SRR is proposed, as shown in Fig. 6(a). The L-shaped structure on the bottom left/right corner (green part in Fig. 6(a)) resonates at ~ 6 GHz, while the one on the top left/right corner (yellow part in Fig. 6(a)) resonates at ~ 9.5 GHz. Thus, the resonance frequency of this decoupling SRR can be easily controlled by changing the size of the T-shaped branch. After the HFSS simulations, the decoupling SRR dimensions are finally determined and illustrated in Table 3, and its S-parameters are shown in Fig. 6(b). From the S-parameters, it is clear that this decoupling SRR can resonate at around 3 GHz, 6 GHz and 9.5 GHz.

Table 3. Dimensions of the decoupling SRR.

Symbol	Parameters (unit: mm)
sra	3
a_1	0.4
a_2	0.3
a_3	0.3
a_4	0.8
b_1	0.6
b_2	3.2
b_3	1.5
b_4	0.5
sw_1	4.9
sw_2	4.4
sw_3	0.2

In Fig. 7(a) and Fig. 7(b), the surface current distributions on the decoupling SRR at 6 and 9.5 GHz are presented, respectively. The surface current distributions show that these two bands are controlled by the T-shaped branch of the decoupling SRR.

In addition, based on the metamaterial theory, the extracted effective parameters are shown in Fig. 8. The extracted parameter results exhibit that the decoupling SRR behaves as MNG at the 1st resonant frequency and ENG at the 2nd and 3rd resonant frequencies which are in accordance with two SRR structure characteristics. The extracted effective parameters can help better applying this decoupling SRR.

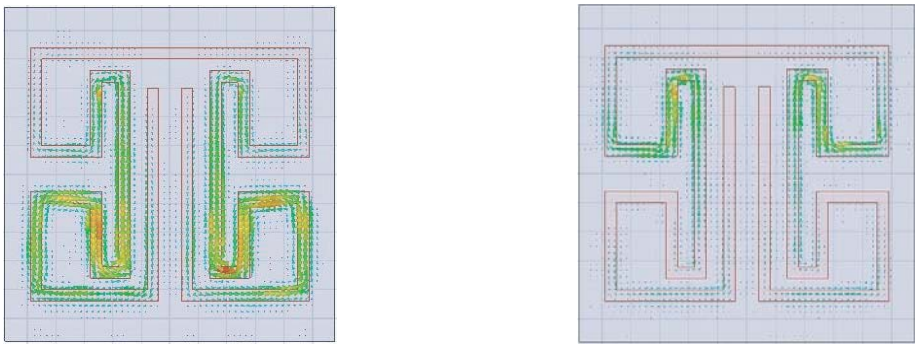

(a) (b)

Figure 7. (a) Surface current distributions on the decoupling SRR at 6 GHz and (b) 9.5 GHz.

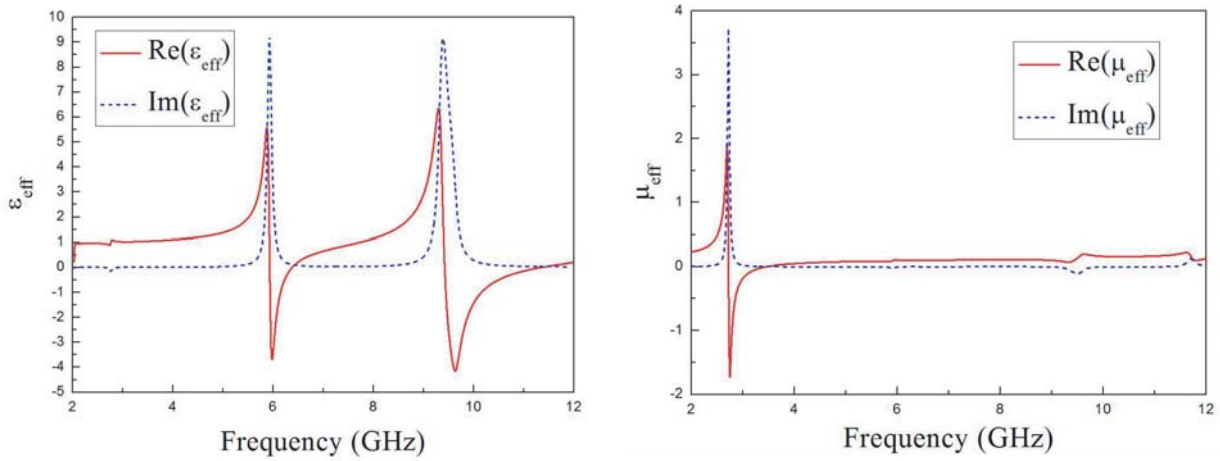

Figure 8. Effective (a) permittivity and (b) permeability of the decoupling SRR.

Using HFSS, a plane is set to observe the magnetic field between two elements, study the coupling effect and determine the best location of the decoupling SRR. According to its extracted effective parameters, the magnetic field at 3 GHz is centred near the bottom of the slot on the surface of the substrate, as shown in Fig. 9(a). This phenomenon implies that the coupling energy between two antenna elements is mainly transported through substrate, not radiation in free space. Besides, the electric field shows a similar property at 6 GHz and 9.5 GHz. Therefore, loading the decoupling SRR on the area C marked in Fig. 9(a) can reduce the coupling effect between the two elements.

The geometry and simulated S-parameters of the antennas with the decoupling SRR are presented in Fig. 9(b) and Fig. 9(c), respectively. From Fig. 9(c), the decoupling SRR is found to significantly decrease $|S_{21}|$ from 3 GHz to 4.5 GHz, and the valley value appears at around 3 GHz where $|S_{21}|$ drops from -6 dB to -34 dB. In the resonant band from ~ 8 GHz to ~ 11 GHz, the isolation has been improved (the $|S_{21}|$ drops from -15 dB to -20 dB).

4. EXPERIMENT AND DISCUSSION

Based on the above simulation and analysis, the UWB MIMO antenna is fabricated and shown in Fig. 10(a). The S-parameters and radiation pattern are measured in an anechoic chamber which is shown in Fig. 10(b). The transmitting antenna is a 3–15 GHz horn antenna and is placed 10 meters away from the UWB MIMO antenna under test.

$|S_{11}|$ and $|S_{21}|$ parameters of the MIMO antenna are measured and presented in Fig. 11(a). The experimental results are in a good agreement with the simulated data at frequencies from 3 GHz to 6 GHz. At frequencies from 6 GHz to 12 GHz, the deviation of the S-parameters is larger. This level of disagreement is predictable since the proximity of the feed network and fabrication errors show stronger influence at higher frequencies. Overall, the measured performance is still in a good agreement with the simulation.

The maximum gain and radiation efficiency of the UWB MIMO antenna are illustrated in Figs. 11(b) and (c), respectively. The figure shows that the UWB MIMO antenna maintains high efficiency (above 70%) in the operating band except the two notch-bands. At frequencies around 3 GHz and 6 GHz, the radiation efficiency slightly decreases due to the proposed isolator as expected. This proves that the proposed isolator is excited by the coupling energy on the substrate with a weak influence on the radiation power in the free space. Notice that the measured efficiency is much lower than the simulation, which is due to the feeding cable adapted in the experiment [32].

To further illustrate the superiority of the proposed structure, the comparison of the proposed UWB MIMO antenna and some latest works are presented in Table 4 (λ_g refers to the wavelength of the lower frequency in the bandwidth). Compared with the previous work, the surface area of the

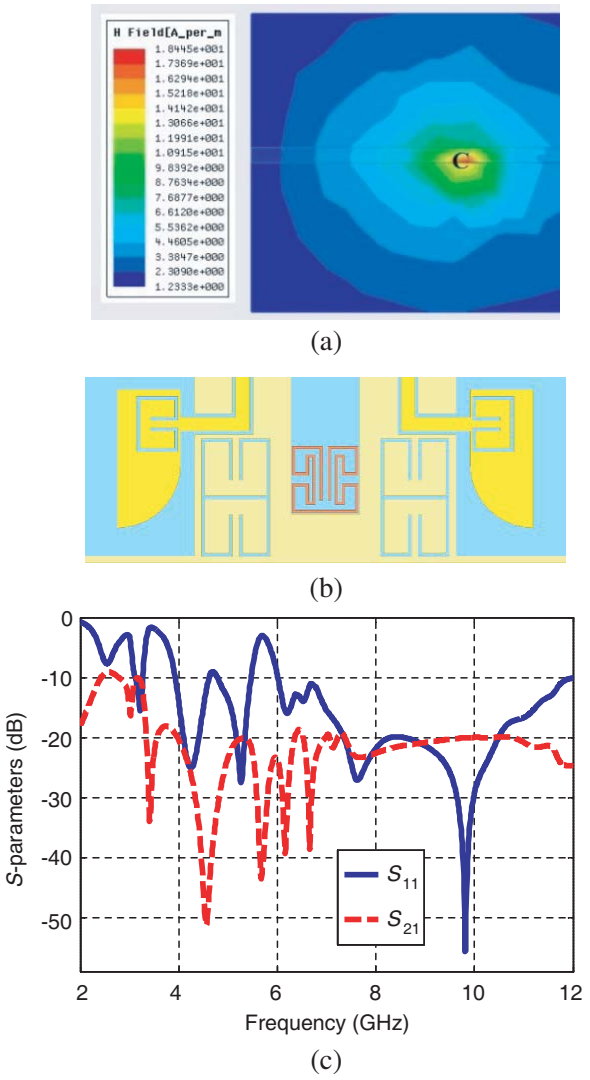

Figure 9. (a) Magnetic field distribution between the two antennas, (b) MIMO antenna with decoupling SRR, (c) its S-parameters.

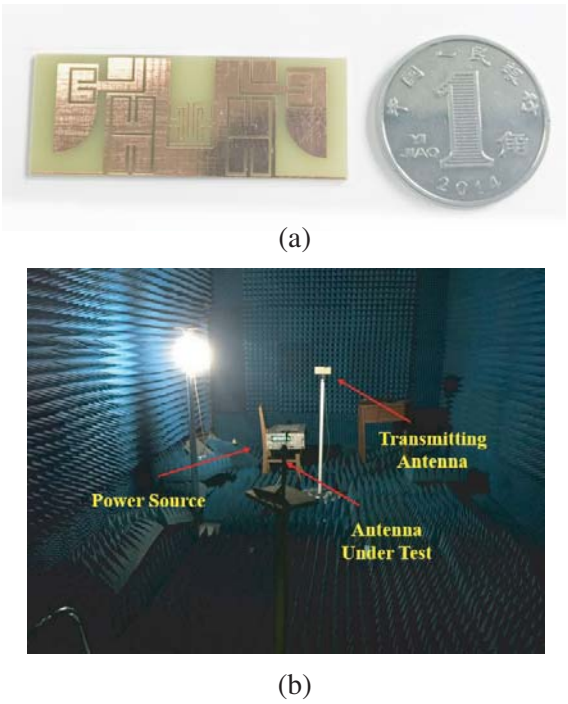

Figure 10. (a) Geometry of the fabricated antenna (b) and the experimental platform.

Table 4. Comparison with the previous work.

Paper	Dimensions	Bandwidth (GHz)	Isolation (dB)	Peak gain (dBi)	ECC	Radiation Efficiency
Ref. [7]	$0.26\lambda_g \times 0.4\lambda_g$	3.1–10.6	≥ 15	5.2	0.1	$> 82\%$
Ref. [8]	$0.55\lambda_g \times 0.55\lambda_g$	2.8–11	≥ 14	6.2	0.01	not given
Ref. [28]	$0.3\lambda_g \times 0.4\lambda_g$	3–11	≥ 16	not given	0.1	$> 72\%$
Ref. [29]	$0.48\lambda_g \times 0.48\lambda_g$	3–11	≥ 17	2	not given	$> 60\%$
Ref. [30]	$0.22\lambda_g \times 0.36\lambda_g$	3–12	≥ 13	4	0.03	$> 70\%$
Ref. [31]	$0.27\lambda_g \times 0.3\lambda_g$	3–11	≥ 20	not given	0.01	$> 30\%$
This paper	$0.135\lambda_g \times 0.34\lambda_g$	3–12	≥ 19	4	0.01 (outside notch band)	$> 60\%$

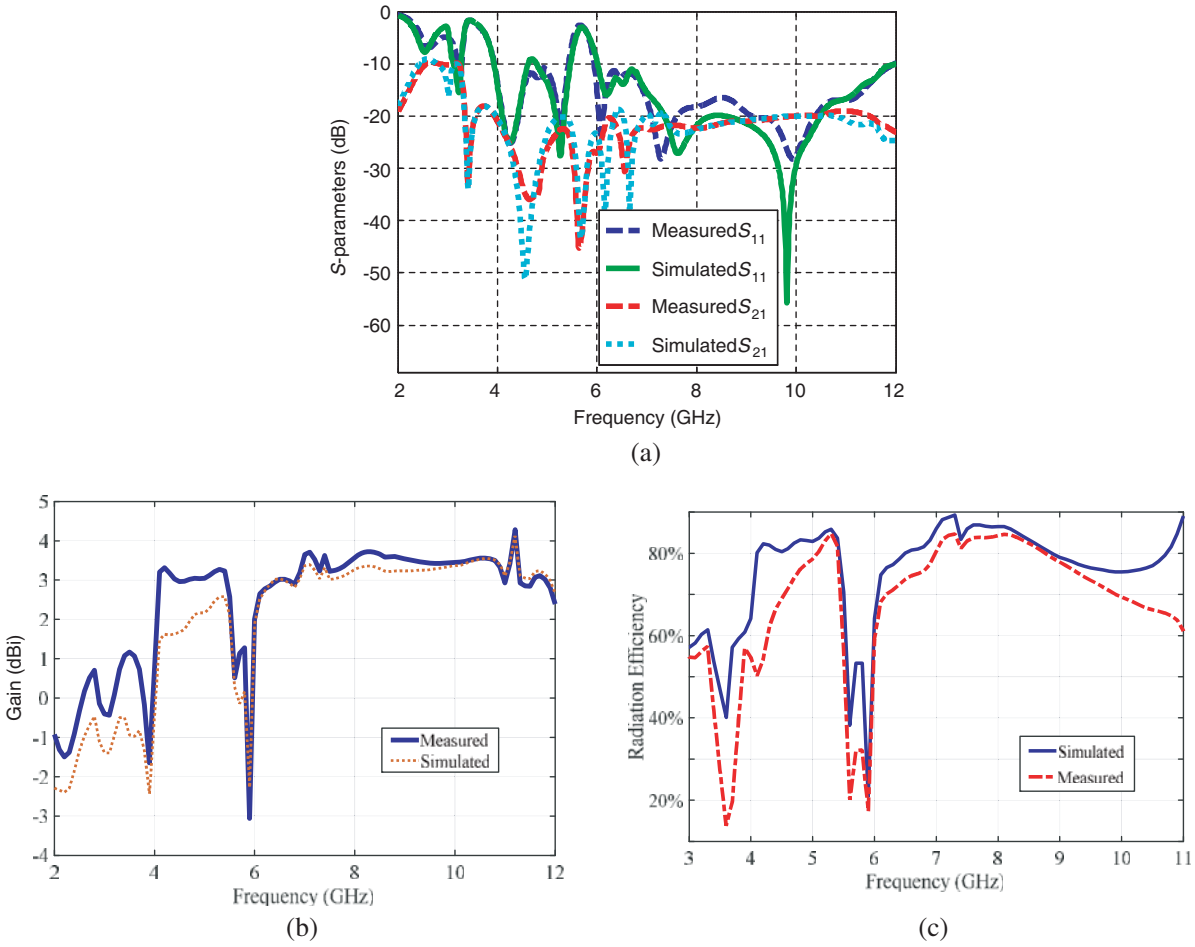

Figure 11. (a) Simulated and measured S-parameters of the UWB MIMO antenna, (b) measured maximum gain and (c) radiation efficiency of the UWB MIMO antenna.

proposed MIMO antenna is smaller than half size of the previous ones, which shows great improvement in miniaturization. Besides, the operation bandwidth of the MIMO antenna has been broadened, and the isolation is higher than most of previous work.

Next, the radiation patterns at 4 GHz and 7 GHz are measured and compared with the simulated results, as shown in Fig. 12. In experiments, the proposed UWB MIMO antenna is used as a receiving antenna. Only one port is connected to the Vector Network Analyser HP8719C, and the other is terminated with 50 Ω matched load.

The radiation patterns from both the simulations and experiments show that the proposed UWB MIMO antenna has an approximate omnidirectional radiation, and the measured results are in good agreement with the simulated ones. Therefore, the proposed UWB MIMO antenna is suitable for cell phones, laptops and other mobile devices.

To compute the radiation performance of the MIMO antenna, the total active reflection coefficient (TARC) is calculated. The TARC can be computed directly from the scattering matrix by using the formula [33]:

$$\Gamma = \frac{\sqrt{\sum_{i=1}^{N} |b_i|^2}}{\sqrt{\sum_{i=1}^{N} |a_i|^2}}, \tag{1}$$

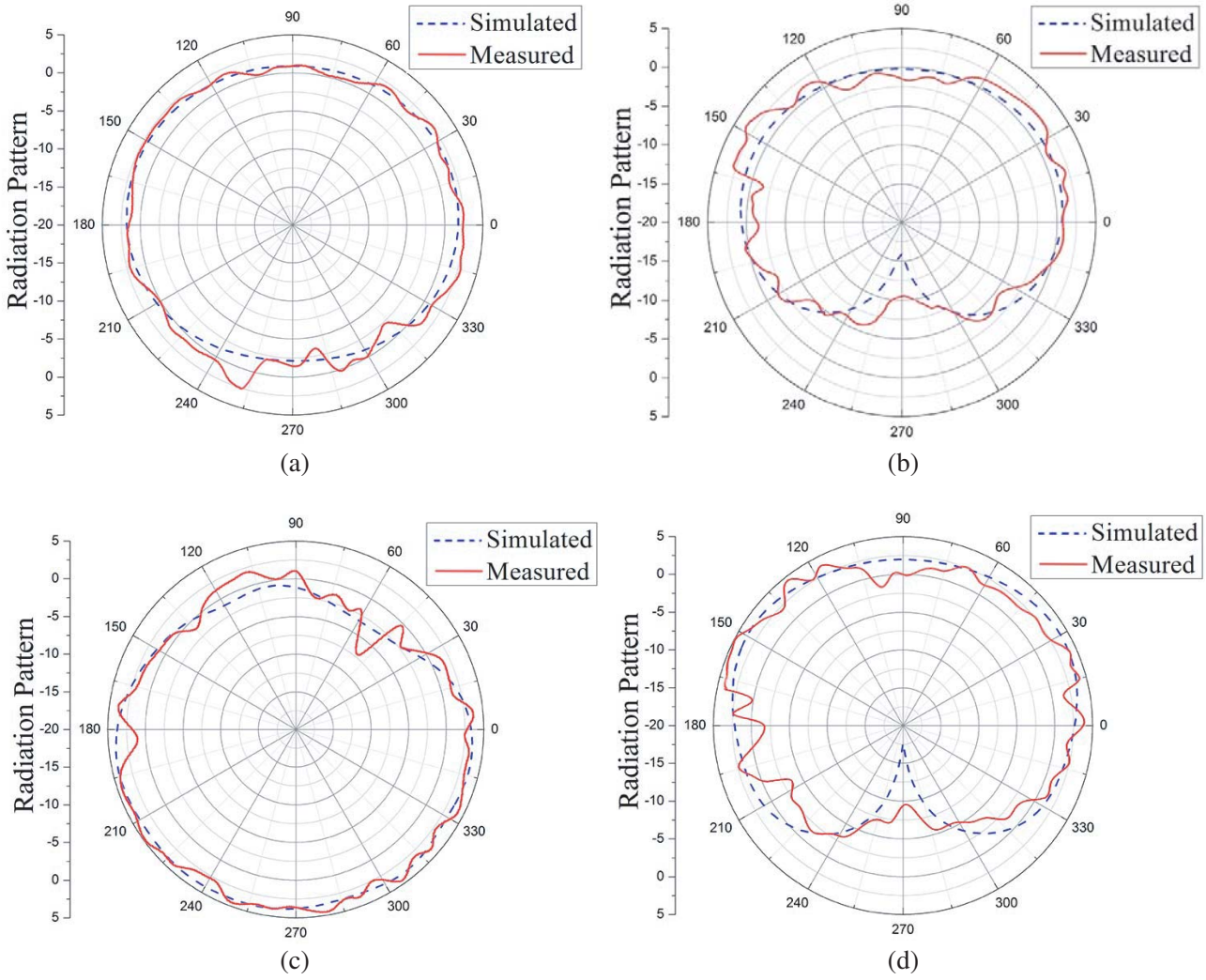

Figure 12. Measured radiation patterns of (a) xz-plane, and (b) yz-plane at 4 GHz, (c) xz-plane and (d) yz-plane at 7 GHz.

where $[b] = [S] \cdot [a]$. $[S]$ is the scattering matrix of the MIMO antenna, $[a]$ the excitation vector, and $[b]$ the scattered vector.

Finally, as an important parameter of the MIMO antenna, the enveloped correlation coefficient (ECC) is used to quantify the isolation among the MIMO antenna elements. ECC is calculated using complex far field patterns over a sphere. Therefore, we use the measured S-parameters and radiation patterns to calculate the ECC [34]:

$$\rho_e = \frac{\left| \iint_{4\pi} \left[\overrightarrow{E_1}(\theta,\phi) \cdot \overrightarrow{E_2}(\theta,\phi) \right] d\Omega \right|^2}{\iint_{4\pi} \left| \overrightarrow{E_1}(\theta,\phi) \right|^2 d\Omega \iint_{4\pi} \left| \overrightarrow{E_2}(\theta,\phi) \right|^2 d\Omega}, \tag{2}$$

where $E_i(\theta,\phi)$ refers to the electric field radiated by antenna element i with the other antenna element terminated by a 50 Ω load. The calculated results are shown in Fig. 14. It can be seen that ρ_e is less than 0.1 in the operation band, which indicates the high isolation between the two antenna elements. Within the operation band, the peak of the ECC appears at around 3.7 GHz and 5.7 GHz. This phenomenon is caused by band-notch C-SRRs which bring extra coupling due to the strong resonances.

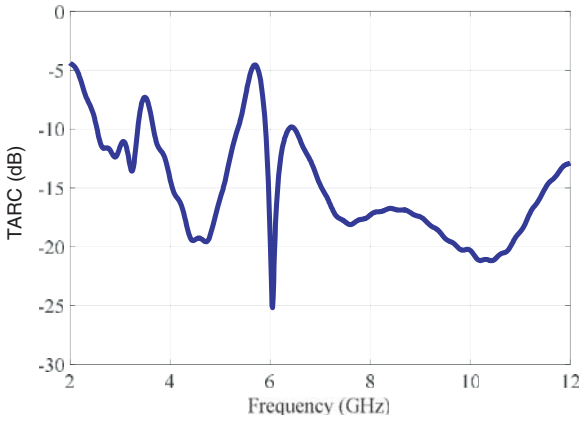

Figure 13. TARC of the proposed UWB MIMO antenna.

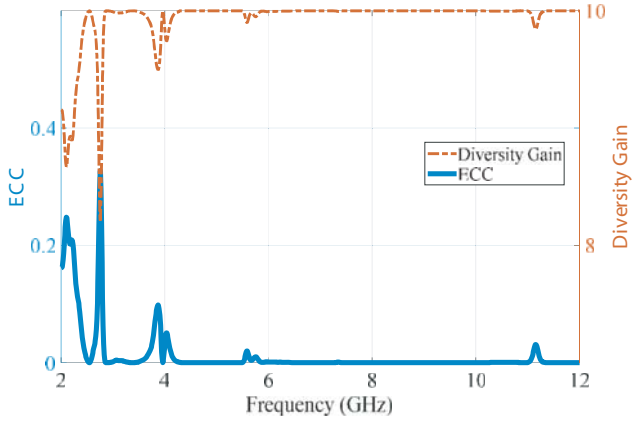

Figure 14. Correlation coefficient and diversity gain of the proposed UWB MIMO antenna.

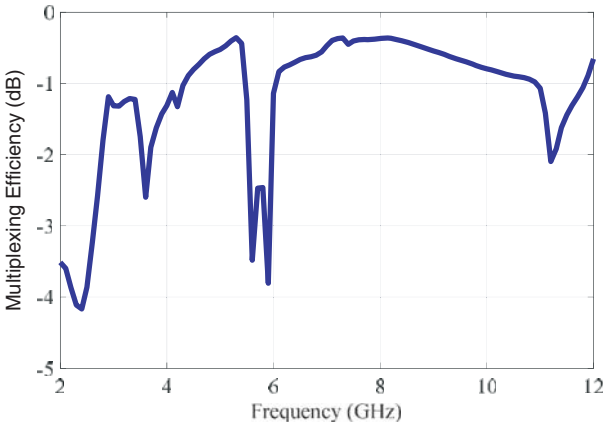

Figure 15. Multiplexing efficiency of the proposed UWB MIMO antenna.

Furthermore, the diversity gain of the proposed MIMO antenna is calculated and presented in Fig. 14. The diversity gain can be computed using the following relation:

$$DG = 10\sqrt{1 - |\rho_e|^2}, \tag{3}$$

Multiplexing efficiency is another important parameter to evaluate the MIMO antenna performance. It can be calculated by using the formula [35]:

$$\eta = \sqrt{(1 - |\gamma|^2)\eta_1\eta_2}, \tag{4}$$

where η_1 and η_2 refer to the measured radiation efficiencies of the two antenna elements, respectively. γ refers to the correlation between antenna elements which can be replaced by the ECC. The calculated multiplexing efficiency is illustrated in Fig. 14. From Fig. 15, it can be seen that the multiplexing efficiency is above -4 dB in the operation band.

5. CONCLUSION

In conclusion, we use a dual-band C-SRR to improve the dual band-notch effect (-2.5 dB at 3.55 GHz and -3 dB at 5.80 GHz). At the same time, we design a novel SRR as an isolator to reduce the coupling in both bands (from ~ 3 GHz to ~ 4 GHz and from ~ 8 GHz to ~ 11 GHz). This metamaterial-inspired isolator can achieve high isolation ($|S_{21}|$ is under -19 dB) and minimization in both bands only using a *single* unit cell. Based on these novel metamaterials, we develop the dual band-notch UWB MIMO

antenna with small size (13.5 mm × 34 mm). The experimental results show that our proposed UWB MIMO antenna has excellent performance such as compact structure, good directivity and high isolation. This metamaterial-inspired UWB MIMO antenna can be used in miniaturized mobile devices.

ACKNOWLEDGMENT

This work was supported in part by the National Natural Science Foundation of China (Grant Nos. 61471091 and 61611130067).

REFERENCES

1. Bolin, T., A. Derneryd, G. Kristensson, et al., "Two antenna receive diversity performance in indoor environment," *Electron. Lett.*, Vol. 41, No. 22, 1205–1206, 2005.
2. Ko, S. C. K. and R. D. Murch, "Compact integrated diversity antenna for wireless communications," *IEEE Trans. Antennas Propag.*, Vol. 49, No. 6, 954–960, 2001.
3. "First report and order in the matter of revision of Part 15 of the Commission's rules regarding ultra-wideband transmission systems FCC," ET-Docket 98-153, 2002.
4. See, T. S. P. and Z. N. Chen, "An ultrawideband diversity antenna," *IEEE Trans. Antennas Propag.*, Vol. 57, No. 6, 1597–1605, 2009.
5. Saraswat, R. K. and M. Kumar, "A frequency band reconfigurable UWB antenna for high gain applications," *Progress In Electromagnetics Research B*, Vol. 64, 29–45, 2015.
6. Rajagopalan, A., G. Gupta, A. S. Konanur, et al., "Increasing channel capacity of an ultrawideband MIMO system using vector antennas," *IEEE Trans. Antennas Propag.*, Vol. 55, No. 10, 2880–2887, 2007.
7. Khan, M. S., A. D. Capobianco, A. L. Najam, I. Shoaib, E. Autizi, and M. F. Shafique, "Compact UWB-MIMO antenna array with a floating digitated decoupling structure," *IET Microw., Antennas & Propag.*, Vol. 8, No. 10, 747–753, 2014.
8. Zhang, S., Z. N. Ying, J. Xiong, et al., "Ultrawideband MIMO/diversity antennas with a tree-like structure to enhance wideband isolation," *IEEE Antennas Wireless Propag. Lett.*, Vol. 8, 1279–1282, 2009.
9. Liu, L., S. W. Cheung, and T. I. Yuk, "Compact MIMO antenna for portable devices in UWB applications," *IEEE Trans. Antennas Propag.*, Vol. 61, No. 8, 4257–4264, 2013.
10. Chacko, B. P., G. Augustin, and T. A. Denidni, "Uniplanar slot antenna for ultrawideband polarization-diversity applications," *IEEE Antennas Wireless Propag. Lett.*, Vol. 12, 88–91, 2013.
11. Iqbal, A., O. A. Saraereh, A. W. Ahmad, and S. Bashir, "Mutual coupling reduction using F-shaped stubs in UWB-MIMO antenna," *IEEE Access*, Vol. 6, 2755–2759, 2018.
12. Duan, Z., B.-I. Wu, J.-A. Kong, F. Kong, and S. Xi, "Enhancement of radiation properties of a compact planar antenna using transformation media as substrates," *Progress In Electromagnetics Research*, Vol. 83, 375–384, 2008.
13. Wang, F., Z. Duan, X. Tang, et al., "Compact high isolation WLAN MIMO antenna based on CRLH," *iWEM 2015*, 1–2, Taipei, China, 2015.
14. Yang, F. and Y. Rahmat-Sami, "Microstrip antennas integrated with electromagnetic band-gap (EBG) structures: A low mutual coupling design for array applications," *IEEE Trans. Antennas Propag.*, Vol. 51, No. 10, 2936–2946, 2003.
15. Yang, L., M. Y. Fan, F. L. Chen, et al., "A novel compact electromagnetic-bandgap (EBG) structure and its applications for microwave circuits," *IEEE Trans. Microw. Theory Tech.*, Vol. 53, No. 1, 183–190, 2005.
16. Rani, M. S. A., S. K. A. Rahim, H. Rezaie, et al., "Directional UWB antenna with a parabolic ground structure and split ring resonator for a 5.80 GHz band notch," *Journal of Electromagnetic Waves and Applications*, Vol. 27, No. 1, 14–22, 2013.

17. Wang, F., Z. Y. Duan, T. Tang, et al., "A new metamaterial-based UWB MIMO antenna," *IEEE IWS 2015*, 1–4, Shenzhen, China, 2015.
18. Saraswat, R. K. and M. Kumar, "Miniaturized slotted ground UWB antenna loaded with metamaterial for WLAN and WiMAX applications," *Progress In Electromagnetics Research B*, Vol. 65, 65–80, 2016.
19. Li, Q., A. P. Feresidis, M. Mavridou, et al., "Miniaturized double-layer EBG structures for broadband mutual coupling reduction between UWB monopoles," *IEEE Trans. Antennas Propag.*, Vol. 63, No. 3, 1170–1173, 2015.
20. Bait-Suwailam, M. M., M. S. Boybay, and O. M. Ramahi, "Electromagnetic coupling reduction in high-profile monopole antennas using single-negative magnetic metamaterials for MIMO applications," *IEEE Trans. Antennas Propag.*, Vol. 58, No. 9, 2894–2902, 2010.
21. Ferrer, P. J., J. M. González-Arbesú, and J. Romeu, "Decorrelation of two closely spaced antennas with a metamaterial AMC surface," *Microw. Opt. Technol. Lett.*, Vol. 50, No. 5, 1414–1417, 2008.
22. Zhu, J., S. Li, S. Liao, and Q. Xue, "Wideband low-profile highly isolated MIMO antenna with artificial magnetic conductor," *IEEE Antennas Wireless Propag. Lett.*, Vol. 17, 458–462, 2018.
23. Ketzaki, D. A. and T. V. Yioultsis, "Metamaterial-based design of planar compact MIMO monopoles," *IEEE Trans. Antennas Propag.*, Vol. 61, No. 5, 2758–2766, 2013.
24. Abdalla, M. A. and A. A. Ibrahim, "Compact and closely spaced metamaterial MIMO antenna with high isolation for wireless applications," *IEEE Antennas Wireless Propag. Lett.*, Vol. 12, 1452–1455, 2013.
25. Khan, M. S., A. -D. Capobianco, S. M. Asif, et al., "A compact CSRR enabled UWB MIMO antenna," *IEEE Antennas Wireless Propag. Lett.*, Vo;. 58, 808–812, 2016.
26. Duan, Z., J. S. Hummelt, M. A. Shapiro, et al., "Sub-wavelength waveguide loaded by a complementary electric metamaterial for vacuum electron devices," *Phys. Plasmas*, Vol. 21, No. 10, 103301, 2014.
27. Pendry, J. B., A. J. Holden, and D. J. Robbins, "Magnetism from conductors and enhanced nonlinear phenomena," *IEEE Trans. Microw. Theory Tech.*, Vol. 47, No. 11, 2075–2084, 1999.
28. Deng, J. Y., L. X. Guo, and X. L. Liu, "An ultrawideband MIMO antenna with a high isolation," *IEEE Antennas Wireless Propag. Lett.*, Vol. 15, 182–185, 2016.
29. Mao, C. X. and Q. X. Chu, "Compact co-radiator UWB-MIMO antenna with dual polarization," *IEEE Trans. Antennas Propag.*, Vol. 62, No. 9, 4474–4480, 2014.
30. Liu, L., S. W. Cheung, and T. I. Yuk, "Compact MIMO antenna for portable UWB applications with band-notched characteristic," *IEEE Trans. Antennas Propag.*, Vol. 63, No. 5, 2015.
31. Li, J. F., Q. X. Chu, Z. H. Li, et al., "Compact dual band-notched UWB MIMO antenna with high isolation," *IEEE Trans. Antennas Propag.*, Vol. 61, No. 9, 4759–4766, 2013.
32. Liu, L., S. W. Cheung, Y. F. Weng, and T. I. Yuk, "Cable effects on measuring small planar UWB monopole antennas," *Ultra Wideband Current Status and Future Trends*, edited by Mohammad Abdul Matin, 2012.
33. Manteghi, M. and Y. Rahmat-Samii, "Multiport characteristics of a wide-band cavity backed annular patch antenna for multipolarization operations," *IEEE Trans. Antennas Propag.*, Vol. 53, No. 1, 466–474, 2005.
34. Hallbjörner, P., "The significance of radiation efficiencies when using S-parameters to calculate the received signal correlation from two antennas," *IEEE Antennas Wireless Propag. Lett.*, Vol. 4, 97–99, 2005.
35. Tian, R., B. K. Lau, and Z. Ying, "Multiplexing efficiency of MIMO antennas," *IEEE Antennas Wireless Propag. Lett.*, Vol. 10, 183–186, 2011.